Chemical Engineering Journal 155 (2009) 371–379

Contents lists available at ScienceDirect

Chemical Engineering Journal

journal homepage: www.elsevier.com/locate/cej

Heat transfer and temperature profiles in flow-through catalytic membrane reactors

Thomas Westermann, Eva Kretzschmar, Fee Pitsch, Thomas Melin*

Aachener Verfahrenstechnik (AVT) - Chemical Process Engineering, RWTH Aachen University, 52056 Aachen, Germany

ARTICLE INFO

Article history:
Received 20 March 2009
Received in revised form 13 July 2009
Accepted 24 July 2009

Keywords:
Catalyst support
Heat transfer
Membranes
Microstructure
Reaction engineering

ABSTRACT

In flow-through membrane reactors, a porous membrane is used as a microstructured catalyst support, which provides for an intensive contact between reactants and catalyst. When performing exothermal gas phase reactions, large temperature differences between feed and permeate side are observed. This work systematically derives an axial temperature profile inside the inaccessible membrane pores by combining a one-dimensional reactor model of mass and energy balances with experimental measurements of reactor temperatures and conversion, applying ethene hydrogenation as a model reaction. It is shown, that the anodized membrane reactor can be regarded as isothermal under any operating conditions and the heat transfer mechanisms inside the membrane prove to be irrelevant for the resulting membrane temperature. By applying the derived heat transfer model to the performed ethene hydrogenation experiments, the reactor temperature can be predicted satisfactorily in the whole range of performed experiments.

1. Introduction

Catalytic porous membranes which are convectively passed by the reaction mixture are frequently called "flow-through catalytic membrane reactors". The porous, mostly ceramic, membrane does not perform any separative task but is solely used as microstructured catalyst support. As the reactor concept allows for a high catalytic activity due to an intensive contact between reactants and catalyst and potentially for a narrow residence time distribution, it has become a popular field of investigation [1–7]. As the reactor length coincides with the membrane thickness, residence times can be smaller than 1 ms, corresponding to space-time-yields in the order of 10^4 mol/m^{3}s.

For strongly exothermal gas phase reactions, such as ethyne or ethene hydrogenation, the adiabatic temperature rise

$$\Delta T_{ad} = \frac{x_{HC} \cdot (-\Delta H_{R,HC})}{c_p} \quad (1)$$

easily reaches 1000 K if operated at low dilution ratios. If these reactions are performed in a flow-through catalytic membrane reactor, the specific thermal load induced by reaction exceeds 1 GW/m^3, leading to large temperature differences of more than 100 K between feed and permeate side [8]. On the other hand, the microstructured geometry causes intensive heat transfer inside the membrane, levelling temperature profiles. The knowledge of the resulting gas and wall temperatures at different sites of the membrane is essential for the calculation of reaction rates and conversions.

This work aims at determining an axial temperature profile along the membrane reactor and corresponding heat transfer coefficients by combining experimental measurements with a non-isothermal reactor model, in order to analyze and predict reactor temperatures under given conditions. All measurements are performed in a flow-through catalytic membrane reactor with the hydrogenation of ethene as model reaction.

2. Materials and methods

2.1. Membrane microstructure

Anodized alumina membranes consist of uniform cylindrical pores and offer a narrow size distribution [9,10]. They are commercially available for microfiltration applications with different nominal pore diameters and a thickness of 60 μm (Whatman Anodisc). SEM images of Whatman Anodisc membranes are given exemplarily in Fig. 1. The top view image of a W02 membrane with a nominal pore diameter of 0.2 μm at a magnification of 10 000 (Fig. 1(a)) illustrates the regular arrangement of open pore channels and the rather narrow size distribution. The cross-section of a W01 membrane with a nominal pore diameter of 0.1 μm at a magnification of 1000 (Fig. 1(b)) demonstrates the pore-channel geometry: the nominal diameter of 0.1 μm can only be found in the thin active layer at the bottom, whereas the main part is made up of channels with diameters around 0.2 μm. The pores are straight and arranged

* Corresponding author. Tel: +49 241 80 95470; fax: +49 241 80 92252.
E-mail address: thomas.melin@avt.rwth-aachen.de (T. Melin).

1385-8947/$ – see front matter © 2009 Elsevier B.V. All rights reserved.
doi:10.1016/j.cej.2009.07.059

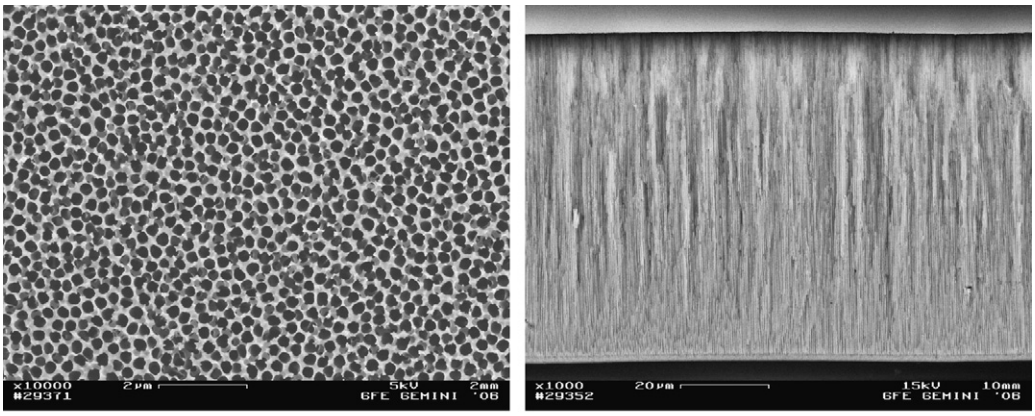

Fig. 1. SEM images of Whatman Anodisc membranes. (a) Top view of W02 membrane, 10 000× magnification and (b) cross-section of W01 membrane with active layer at the bottom, 1000 × magnification.

perpendicular to the surface without bifurcations. Moreover, they are slightly cone-shaped rather than exactly cylindrical. W02 membranes consist of only one uniform layer made up of channels with diameters around 0.2 μm. Because of their uniformity in structure, experiments are performed with W02 membranes. The thickness of the commercially available membranes varies. In the case of the illustrated W01 sample, the thickness is 80 μm instead of 60 μm as given in the specifications by the supplier.

The nano-scale porous structure of anodized alumina membranes promises a highly efficient heat transfer across the gas–wall interface, whereas the limited external surface area of the almost two-dimensional flat sheet membrane does not allow for heat removal in radial direction. On the feed side, the membrane can be considered to be exclusively in contact with the feed gas. However, on the permeate side, heat can be transferred to a porous metal support and further to the external surface of the reactor module (Fig. 2).

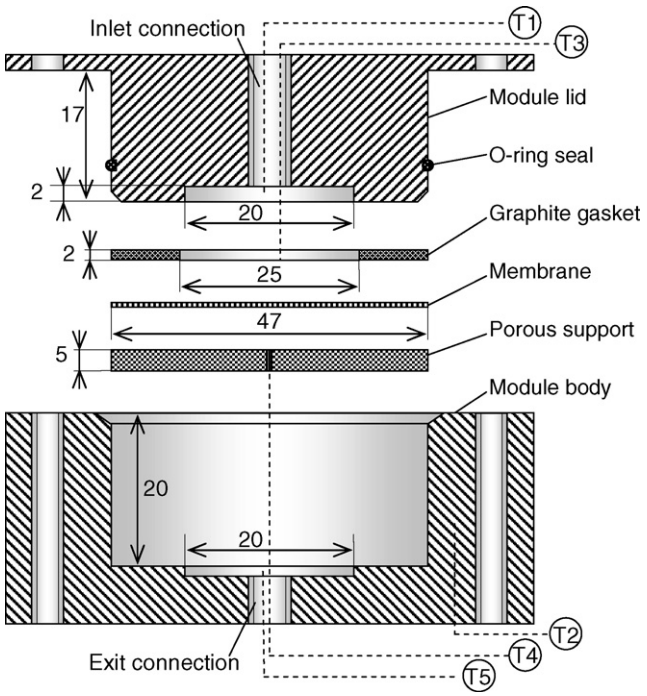

Fig. 2. Reactor module employed for flow-through experiments (dimensioning in mm).

2.2. Experimental setup and procedure

Ethene hydrogenation experiments are performed in a catalytic membrane with a nominal pore diameter of 0.2 μm (W02), placed in a module consisting of a bottom part (body), a porous support plate, a graphite gasket and a top part (lid), as displayed in Fig. 2. The body provides an outlet connection for the product gas flow and a circular cavity for a porous metal support plate, the membrane itself and the module lid. The catalytic membrane is placed on top of the support plate, followed by a graphite gasket with a thickness of 2 mm. A hole in the center of the support plate allows for insertion of a thermocouple to measure the gas temperature on the product side. The lid of the module is equipped with an inlet connection for the feed gas flow and an outside sealing O-ring (FKM 80) to seal the gap between lid and bottom part. It is mounted to the body by means of four socket screws.

Ethene conversion and reactor temperature are measured under variation of flow rate and nitrogen dilution. The feed is a gas mixture of nitrogen and a stoichiometric mixture of the reactants ethene and hydrogen. The detectable reactant concentrations of hydrocarbons are measured in-line by means of Fourier transform infrared spectroscopy (FTIR). The total amount of detected hydrocarbons corresponds to the initial amount of ethene. The concentrations of hydrogen and nitrogen are calculated by a stoichiometric balance. The reactor temperature is measured by thermocouples introduced via the inlet and outlet fittings.

2.3. Reactor model

Compared to conventional reactors, microstructured reactors outstand by their increased heat and mass transfer properties. On the one hand, heat transfer across a gas–wall interface $\dot{Q}_{\text{trans}}$ is proportional to the temperature difference between gas and wall, the surface area of the interface A_{transfer} and a heat transfer coefficient h according to

$$\dot{Q}_{\text{trans}} = h \cdot A_{\text{transfer}} \cdot \left(T_{\text{gas}} - T_{\text{wall}}\right). \quad (2)$$

On the other hand, heat generation of a chemical reaction is proportional to the reactor volume or in case of heterogeneous reactions to the amount of catalyst. By reducing the diameter of a channel, the ratio between channel surface and volume increases, leading to improved heat transfer. However, even more important is another effect. For a constant Nusselt number, describing the ratio between heat transfer and heat conduction, the heat transfer coefficient h is inversely proportional to the channel

diameter d, leading to extremely high heat transfer coefficients in microstructured reactors. Additionally, strong diffusive radial mixing efficiently counteracts concentration or temperature profiles [11]. Thus, despite the laminar flow profile always present in microchannels, a one-dimensional plug flow behavior can be assumed.

Assuming identical pores, the investigated model system can be reduced to a single pore and the surrounding pore wall, with symmetry in radial direction. Furthermore, for small radial concentration gradients inside the pore in consequence of intensive radial mixing, a quasi-homogeneous reaction with plug flow can be assumed [12]. The plug flow assumption reduces the complexity to a single dimension, in which gas temperature, wall temperature and gas composition will be treated as separate variables. Pressure drop is neglected and fluid properties are assumed to be constant along the reactor. Especially for high axial velocities, low absolute pressures, low dilution and high conversion, this is a major simplification, as strong pressure and velocity gradients may arise. Nevertheless, neglecting these parameters allows to focus on heat transfer processes and should at least leads to qualitative correlations.

2.3.1. Material balance

A steady state differential material balance of ethene yields:

$$\frac{\mathrm{d}X_{\mathrm{C_2H_4}}}{\mathrm{d}Z} = -\frac{r_{\mathrm{C_2H_4}}}{x_{\mathrm{C_2H_4,feed}}} = \frac{m_{\mathrm{cat}}}{\dot{n}_{\mathrm{tot}}} k \cdot p^n \cdot x_{\mathrm{C_2H_4,feed}}^{(n-1)} \cdot (1 - X_{\mathrm{C_2H_4}})^n. \tag{3}$$

This equation implies the conversion of ethene $X_{\mathrm{C_2H_4}}$ with the simplification

$$X_{\mathrm{C_2H_4}} = 1 - \frac{\dot{n}_{\mathrm{C_2H_4}}}{\dot{n}_{\mathrm{C_2H_4,feed}}} \approx 1 - \frac{x_{\mathrm{C_2H_4}}}{x_{\mathrm{C_2H_4,feed}}}. \tag{4}$$

Reaction kinetics are incorporated in a dimensionless term, assuming constant pressure and molar flow rate

$$r_{\mathrm{C_2H_4}} = -\frac{m_{\mathrm{cat}}}{\dot{n}_{\mathrm{tot}}} \cdot k \cdot \left(p_{\mathrm{C_2H_4,feed}} \left(1 - X_{\mathrm{C_2H_4}}\right)\right)^n. \tag{5}$$

Assuming a uniform catalyst distribution in the membrane, the values of catalyst mass and molar flow can be given for the whole membrane, rather than for a single pore, as their ratio stays constant.

2.3.2. Gas phase energy balance

To determine axial profiles of the gas and pore wall temperature, two separate energy balances are applied, which are coupled by the heat transfer term between gas and pore wall. In both balances all radial profiles are neglected. A steady state differential energy balance for a volume element $\mathrm{d}V = A \cdot \mathrm{d}z$ takes into account the convective heat transfer $\dot{Q}_{\mathrm{conv}}$ into and out of the control volume, heat conduction $\dot{Q}_{\mathrm{cond}}$ in and against flow direction, heat transfer between the gas and pore wall $\dot{Q}_{\mathrm{trans}}$ and heat generation by a chemical reaction $\dot{Q}_{\mathrm{react}}$. The effective axial heat conduction incorporates all axial mixing processes [13]:

$$-\frac{\partial \dot{Q}_{\mathrm{conv}}}{\partial z}\,\mathrm{d}z - \frac{\partial \dot{Q}_{\mathrm{cond}}}{\partial z}\,\mathrm{d}z - \dot{Q}_{\mathrm{trans}} + \dot{Q}_{\mathrm{react}} = 0. \tag{6}$$

The single terms can be calculated as follows:

$$\dot{Q}_{\mathrm{conv}} = \dot{n}_{\mathrm{tot}} \cdot c_p \cdot T, \tag{7}$$

$$\dot{Q}_{\mathrm{cond}} = -A \cdot k_{\mathrm{gas}} \cdot \frac{\partial T_{\mathrm{gas}}}{\partial z}, \tag{8}$$

$$\dot{Q}_{\mathrm{trans}} = h \cdot (T_{\mathrm{gas}} - T_{\mathrm{wall}}) \cdot \pi d \cdot \mathrm{d}z, \tag{9}$$

$$\dot{Q}_{\mathrm{react}} = \Delta H_{\mathrm{R}} \cdot \dot{n}_{\mathrm{tot}} \cdot \frac{\partial x_{\mathrm{C_2H_4}}}{\partial z} \cdot \mathrm{d}z. \tag{10}$$

Introducing a dimensionless length $Z = z/L$ and temperature $\Theta = T/T_0$ as well as the ethene conversion according to Eq. (4), several parameters can be cropped, forming dimensionless quantities.

The Nusselt number

$$Nu = \frac{h \cdot \pi d L^2}{A \cdot k_{\mathrm{gas}}} \tag{11}$$

describes the ratio between heat transfer and heat conduction in the gas phase. It is important to note that heat transfer is proportional to the pore wall surface πdL, whereas heat conduction is proportional to the cross-section area of the pore $A = \pi/4d^2$.

The Péclet number

$$Pe = \frac{\dot{n} \cdot c_p \cdot L}{A \cdot k_{\mathrm{gas}}} \tag{12}$$

characterizes the ratio between heat convection and heat conduction in the gas phase.

The dimensionless adiabatic temperature difference

$$\Delta\Theta_{\mathrm{ad}} = -\frac{\Delta H_{\mathrm{R}} \cdot x_{\mathrm{C_2H_4,feed}}}{c_p \cdot T_0} \tag{13}$$

is normalized to the reference temperature T_0.

The energy balance for the gas phase results as:

$$\frac{\mathrm{d}^2\Theta_{\mathrm{gas}}}{\mathrm{d}Z^2} = Pe \cdot \frac{\mathrm{d}\Theta_{\mathrm{gas}}}{\mathrm{d}Z} + Nu \cdot \left(\Theta_{\mathrm{gas}} - \Theta_{\mathrm{wall}}\right) - Pe \cdot \Delta\Theta_{\mathrm{ad}} \cdot \frac{\mathrm{d}X_{\mathrm{C_2H_4}}}{\mathrm{d}Z}. \tag{14}$$

2.3.3. Pore wall energy balance

The accessible membrane area A_{mem} can be subdivided into a total pore area $A_{\mathrm{mem,pore}}$ and a total wall area $A_{\mathrm{mem,wall}}$ according to the porosity ϵ:

$$A_{\mathrm{mem}} = A_{\mathrm{mem,pore}} + A_{\mathrm{mem,wall}} = \epsilon \cdot A_{\mathrm{mem}} + (1 - \epsilon) \cdot A_{\mathrm{mem}}. \tag{15}$$

The cross-sectional area of wall material A_{wall} of a single pore, which is characteristic for heat conduction, is calculated by allocating the same amount of wall material to each pore according to

$$A_{\mathrm{wall}} = \frac{1 - \epsilon}{\epsilon} \cdot A, \tag{16}$$

assuming identical heat transfer characteristics in each pore and thus no radial heat transfer between pore walls (Fig. 3).

The steady state differential energy balance for a volume element of the pore wall $\mathrm{d}V_{\mathrm{wall}} = A_{\mathrm{wall}} \cdot \mathrm{d}z$ takes into account heat conduction $\dot{Q}_{\mathrm{cond}}$ in and against flow direction and heat transfer between gas and pore wall $\dot{Q}_{\mathrm{trans}}$:

$$-\frac{\partial \dot{Q}_{\mathrm{cond}}}{\partial z}\,\mathrm{d}z + \dot{Q}_{\mathrm{trans}} = 0. \tag{17}$$

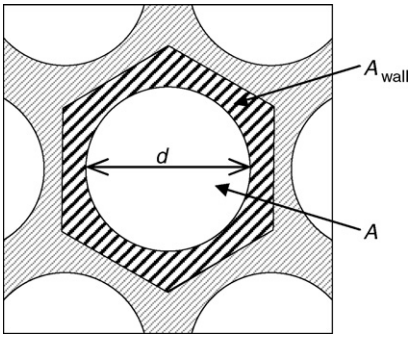

Fig. 3. Axial membrane cross-section with pore area A and allocated wall area A_{wall}.

Note that in contrast to the gas phase energy balance, heat transfer is here declared as positive. The single terms can be calculated as follows:

$$\dot{Q}_{\text{cond}} = -\frac{1-\epsilon}{\epsilon} \cdot A \cdot k_{\text{wall}} \cdot \frac{\partial T_{\text{wall}}}{\partial z} \tag{18}$$

$$\dot{Q}_{\text{trans}} = h \cdot (T_{\text{gas}} - T_{\text{wall}}) \cdot \pi d \cdot \mathrm{d}z. \tag{19}$$

Again, a dimensionless quantity can be introduced. The Biot number

$$Bi = \frac{\epsilon}{1-\epsilon} \frac{h \cdot \pi d L^2}{A \cdot k_{\text{wall}}} \tag{20}$$

characterizes the ratio between heat transfer and heat conduction in the pore wall. Heat transfer is proportional to the pore wall surface πdL, whereas heat conduction is proportional to the allocated cross-section area of the pore wall A_{wall} as described in Eq. (16).

The energy balance for the pore wall results as:

$$\frac{\mathrm{d}^2\Theta_{\text{wall}}}{\mathrm{d}Z^2} = -Bi \cdot \left(\Theta_{\text{gas}} - \Theta_{\text{wall}}\right). \tag{21}$$

2.3.4. Boundary conditions

The reactor model consists of the three coupled differential Eqs. (3), (14) and (21) with the variables $X_{C_2H_4}$, Θ_{gas} and Θ_{wall}. The energy balances are second order differential equations and the material balance is of first order. This leads to a boundary value problem, requiring five boundary conditions.

The boundary condition for the material balance is rather simple, as the conversion of ethene is assumed to be zero at the pore entrance since axial dispersion is neglected

$$X_{C_2H_4}(Z=0) = 0. \tag{22}$$

Energy balances at the pore entrance for both gas phase and pore wall lead to the well-known boundary conditions proposed by Danckwerts [14]

$$\Theta_{\text{gas}}(Z=0) = 1 + \frac{1}{Pe} \cdot \frac{\mathrm{d}\Theta_{\text{gas}}}{\mathrm{d}Z}(Z=0), \tag{23}$$

$$\Theta_{\text{wall}}(Z=0) = 1 + \frac{1}{Bi_0} \cdot \frac{\mathrm{d}\Theta_{\text{wall}}}{\mathrm{d}Z}(Z=0). \tag{24}$$

They allow for a temperature step between feed temperature T_0 and gas and wall temperatures at $Z = 0$. As the feed temperature is chosen as reference temperature, the dimensionless feed temperature $\Theta_{\text{feed}} = 1$ appears in the boundary conditions.

For the pore wall energy balance, a Biot number for the pore entrance

$$Bi_0 = \frac{h_0 \cdot L}{k_{\text{wall}}} \tag{25}$$

appears as additional dimensionless quantity, which differs from the Biot number defined in Eq. (20) not only by the characteristic length, but also by the heat transfer coefficient h_0, as the heat transfer characteristics are different inside a channel and at the front face of the channel.

The remaining two boundary conditions define the heat transfer behavior at the pore outlet. Two different models are discussed at this stage, labelled model 1 and model 2, respectively. As a first assumption (model 1), temperature steps similar to those at the entrance are allowed at the outlet. This assumption is feasible, if the catalytic membrane is cooled from the outlet side. The corresponding boundary conditions completing model 1 are

$$\Theta_{\text{gas}}(Z=1) = \Theta_{\text{permeate}} - \frac{1}{Pe} \cdot \frac{\mathrm{d}\Theta_{\text{gas}}}{\mathrm{d}Z}(Z=1), \tag{26}$$

$$\Theta_{\text{wall}}(Z=1) = \Theta_{\text{permeate}} - \frac{1}{Bi_1} \cdot \frac{\mathrm{d}\Theta_{\text{wall}}}{\mathrm{d}Z}(Z=1). \tag{27}$$

The Biot number at the pore outlet Bi_1 is defined correspondingly to Eq. (25). It has to be noted that the dimensionless permeate temperature is not known if the model is predictive.

If the gas and wall temperature at the pore outlet are close to the permeate temperature, heat conduction as well as heat transfer from the pore wall to the reactor module can be neglected (model 2). In this case, the temperature gradients at $Z = 1$ turn to zero, yielding the classical Danckwerts boundary conditions at the outlet, completing model 2:

$$\frac{\mathrm{d}\Theta_{\text{gas}}}{\mathrm{d}Z}(Z=1) = 0, \tag{28}$$

$$\frac{\mathrm{d}\Theta_{\text{wall}}}{\mathrm{d}Z}(Z=1) = 0. \tag{29}$$

This assumption is a severe simplification, especially if the catalytic membrane is actively cooled. The two models differ in the temperature gradients allowed at the outlet. Nevertheless, both of them are suitable to describe the reactor behavior under the applied experimental conditions, as will be demonstrated for model 2. They even lead to identical temperature profiles. Thus, in the following, only the results of model 2 will be presented for reasons of convenience. It does not require knowledge of the permeate temperature, neither of the additional parameter Bi_1, implying that all heat removal is attributed to Bi_0.

3. Results and discussion

3.1. Reaction kinetics

Applying a catalytic anodized membrane with a palladium content of 0.14 mg, ethene hydrogenation experiments are performed, measuring ethene conversion and reactor temperature, under variation of flow rate and nitrogen dilution. All experiments are carried out with stoichiometric feed of the reactants ethene and hydrogen, with the result that their concentrations are equal at all times. This procedure does not allow for exact determination of the reaction kinetics, but it reduces the number of kinetic parameters as the two individual reaction orders of ethene and hydrogen can be replaced by a total reaction order. Applying an Arrhenius expression for temperature dependence, a three parameter kinetic rate law is supposed (Eq. (30)). The kinetic parameters are determined from the experimentally measured conversions assuming isothermal ideal plug flow behavior, so assuming the temperature of the product being the constant reactor temperature. This assumption will be validated in Section 4.

$$r_{C_2H_4} = -k_\infty \exp\left(\frac{-E_A}{RT}\right) p^n_{C_2H_4} \tag{30}$$

$$n = 1.8 \tag{31}$$

$$k_\infty = 3.75 \times 10^4 \,\text{mol}/(\text{kg}_{\text{cat}}\,\text{s}\,\text{bar}^n) = 3.75 \times 10^{-5} \,\text{mol}/(\text{kg}_{\text{cat}}\,\text{s}\,\text{Pa}^n) \tag{32}$$

$$E_A = 2\,001\,\text{J/mol}. \tag{33}$$

The best agreement between experiment and model is reached for a reaction order of $n = 1.8$. The determined activation energy of $E_A = 2\,001$ J/mol is rather low. Compared to the reaction kinetics given in Ref. [15] with a corresponding value of $E_A = 40\,600$ J/mol, determined for higher dilutions and at lower temperatures, the temperature influence is much less significant. The total reaction order of 1.8 on the other hand is much higher than the value of $1.45 - 0.85 = 0.6$ reported in Ref. [15]. Comparing initial reaction rates for the applied experimental parameters calculated with both rate laws, the determined reaction rate per catalyst mass is faster by a factor of 3 (for $T = 572$ K) up to 65 (for $T = 410$ K). A role of nitrogen in the reaction kinetics cannot be excluded. Nitrogen could

Table 1
Ethene hydrogenation kinetics: reaction conditions and measured conversions compared to model predictions.

$x_{C_2H_4}$	Q_{tot} [l_N/min]	$Q_{C_2H_4}$ [l_N/min]	p_{feed} [$\times 10^5$ Pa]	T [K]	X_{exp}	X_{sim}
0.50	0.80	0.40	1.00	572	0.77	0.80
0.50	1.50	0.75	1.03	537	0.67	0.67
0.50	2.50	1.25	1.09	477	0.51	0.54
0.40	1.00	0.40	1.02	531	0.71	0.71
0.40	1.88	0.75	1.06	505	0.60	0.57
0.40	3.13	1.25	1.15	454	0.47	0.46
0.33	1.20	0.40	1.04	481	0.62	0.63
0.33	2.25	0.75	1.11	466	0.52	0.49
0.33	3.75	1.25	1.24	429	0.41	0.40
0.29	1.40	0.40	1.06	447	0.55	0.56
0.29	2.63	0.75	1.16	433	0.45	0.43
0.29	4.38	1.25	1.34	410	0.34	0.36

compete with the reactants for adsorption sites at the catalyst and thus reduces the overall reaction rate, although no site competition with nitrogen has been reported for Pd-catalyzed hydrogenation reactions. Small traces of CO in the nitrogen 5.0 gas cylinder could also cause the decrease of reaction kinetics at higher nitrogen dilution [16]. As the experimental conditions are not comparable and the power law kinetics are only valid in a small region of operating parameters, this result is no conclusive evidence regarding increased catalytic activity.

Table 1 shows the applied operating conditions of the performed experiments. In addition to the experimentally measured conversions X_{exp}, the theoretical conversions X_{sim} are displayed, which are calculated by applying the determined kinetic parameters to the plug flow reactor model. The agreement is rather good with maximum deviations of 3%.

3.2. Heat transfer model parameter study

The general model derived in Section 2.3 allows for different temperature profiles, depending on the numerical values of the model parameters. The developed reactor model includes the dimensionless quantities *Nu*, *Pe* and *Bi* as parameters, which are functions of material properties and operating parameters and can thus be calculated in advance. The unknown parameter Bi_0 characterizes the heat removal from the membrane.

As an exemplary result, Fig. 4 shows the resulting profiles for the case that all dimensionless parameters are equal to one. This means that the heat transfer in the pore is equal to the heat transfer on the feed side, to the heat conduction in the gas phase, to the heat conduction in the pore wall and to the heat convection. No heat transfer is assumed on the permeate side according to Section 2.3. These conditions do not represent a specific point of operation of the investigated reactor, but demonstrate the general profiles and the influence of the single parameters.

The dimensionless feed temperature is defined to be $\Theta_{feed} = 1$. The resulting temperature jump at the reactor inlet from $\Theta_{feed} = 1$ to $\Theta_{gas}(Z = 0) = 2.8$ (Fig. 4) is very pronounced and proportional to the temperature gradient at the same point according to Eq. (23). The wall temperature is far below the gas temperature, but well above the feed temperature. At $Z = 1$, both temperature gradients turn to zero, as defined in Eqs. (28) and (29). The gas temperature increases by 59% of the adiabatic temperature rise, signifying that 41% of the generated heat is removed from the reactor.

In Fig. 5 the same model is calculated four times, varying only one of the four parameters *Pe*, *Nu*, *Bi* and Bi_0. In each case the respective parameter is set to 10. For equal catalyst concentration, the conversion is a function of the total flow rate, which is proportional to *Pe*. For better comparability this proportionality is neglected by assuming an adjusted catalyst mass,

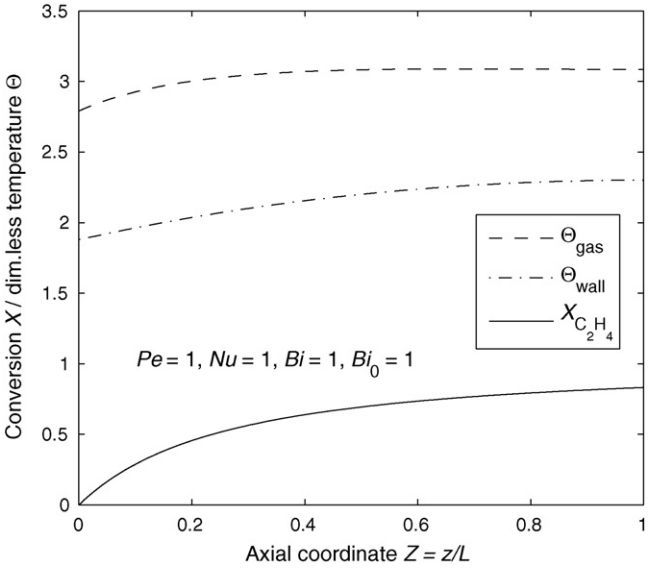

Fig. 4. Axial profiles of conversion, gas and wall temperature for $T_{feed} = 387$ K, $p = 10^5$ Pa, $Q_{tot} = 0.8\,l_N$/min and $x_{C_2H_4} = 0.5$.

leading to comparable conversions and thus comparable heat generation.

The case $Nu = 10$ signifies that internal heat transfer between gas and pore walls is intensified compared to heat conduction in the gas. Due to mutual dependence of the dimensionless quantities, this implies intensified heat transfer on the feed side and heat conduction in the pore wall compared to heat convection. Due to a good heat conduction in the solid, a nearly isothermal profile of the wall temperature is achieved. The intensified heat transfer in the pore does not allow for large temperature differences between pore wall and gas phase. The result is a much smaller difference between gas and wall temperature at a much lower level compared to Fig. 4. The gas temperature reaches a maximum shortly after the reactor inlet, where heat generation is still high but the influence of heat removal on the feed side has decreased. 87% of the generated heat is removed from the reactor.

The case $Pe = 10$ corresponds to intensified heat convection compared to heat conduction in the gas phase as well as to internal and external heat transfer and heat conduction in the pore wall. Only 20% of the generated heat is removed from the reactor, leading to very high gas temperatures close to the adiabatic temperature. The poor conductivities generate pronounced temperature profiles. For a very short interval at the reactor inlet, the wall temperature is even slightly higher than the gas temperature due to heat conduction in the pore wall from the warmer zones in the rest of the reactor.

For $Bi = 10$, internal heat transfer in the pore is intensified compared to heat conduction in the pore wall. This implies intensified heat convection and heat conduction in the gas phase compared to external heat transfer on the feed side. Similar to the case $Nu = 10$ the intensive heat transfer in the pore accounts for a small temperature difference between gas and wall. The heat removal rate on the other hand is with only 22% much smaller due to the reduced heat transfer on the feed side. The temperature jump at the reactor inlet is the most pronounced of all cases.

Finally, $Bi_0 = 10$ signifies that the external heat transfer on the feed side is intensified compared to heat conduction in the pore wall, as well as to heat conduction in the gas phase, heat convection and internal heat transfer. Nevertheless the heat removal rate is rather low with a value of 52%, due to poor internal heat transfer from gas phase to pore wall. The dimensionless wall

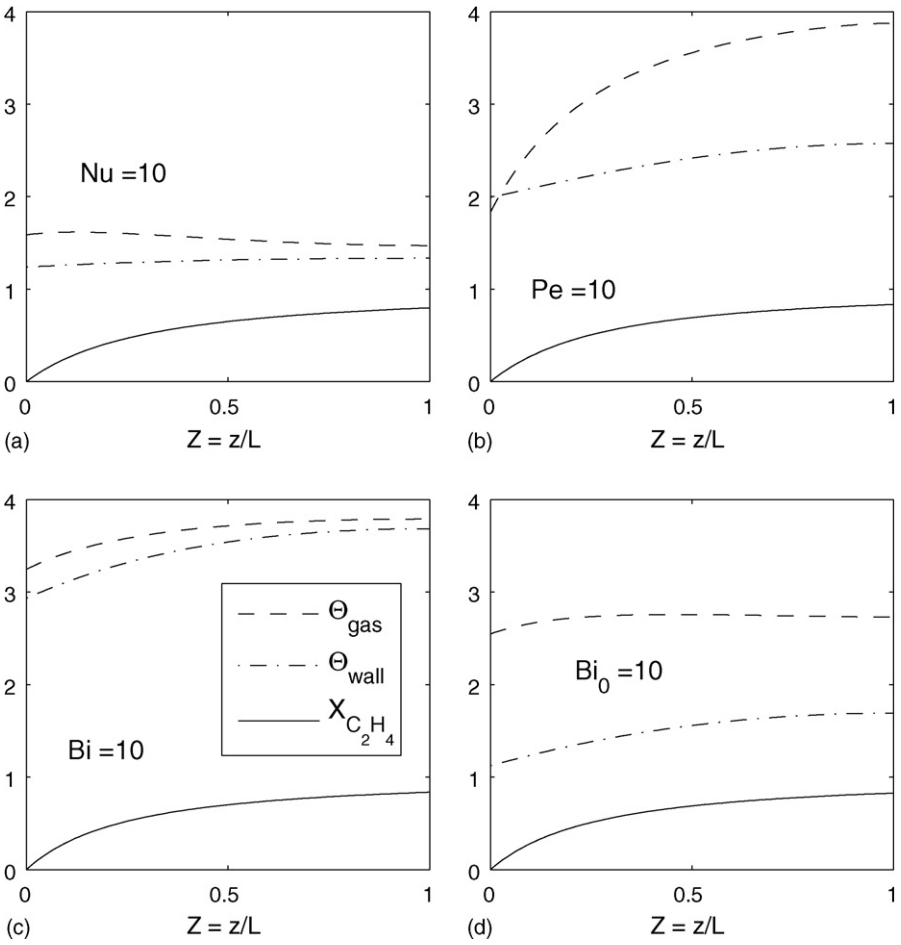

Fig. 5. Influence of model parameters on axial profiles of conversion, gas and wall temperature for $T_{feed} = 387$ K, $p = 10^5$ Pa, $Q_{tot} = 0.8\,l_N/min$ and $x_{C_2H_4} = 0.5$. (a) $Nu = 10$, $Pe = Bi = Bi_0 = 1$ and (b) $Pe = 10$, $Nu = Bi = Bi_0 = 1$; amount of catalyst increased to compensate for reduced residence time, (c) $Bi = 10$, $Nu = Pe = Bi_0 = 1$ and (d) $Bi_0 = 10$, $Nu = Pe = Bi = 1$.

temperature at $Z = 0$ is close to 1, but the difference between gas and wall temperature is comparable to the one displayed in Fig. 4.

The discussion demonstrates that for a given system, the parameters cannot be varied independently. Each of the four dimensionless quantities significantly influences the temperature profiles. For an assessment of the real reactor behavior, reasonable ranges for the parameter values are determined.

3.3. Heat transfer coefficient and Nusselt number

The heat transfer coefficient h, which appears in the dimensionless quantities Nu and Bi, represents the proportionality factor for heat transfer between gas and pore wall. For various conditions it can be calculated by means of Nusselt correlations. For laminar flow-through a circular channel assuming constant wall temperature, the mean Nusselt number $\overline{Nu}_d = h \cdot d/k_{gas}$ is a function of the factor $Re \cdot Pr \cdot d/L$ [17]. For very low Reynolds numbers present in sub-micron channel diameters, the factor becomes very small and the correlation asymptotically reaches the value $Nu_d = 3.66$ [11]. With an assumed Reynolds number in the region of 2×10^{-3} to 2×10^{-2}, which is calculated based on a density of 1 kg/m^3, a velocity of 0.1–1 m/s, a characteristic dimension of 2×10^{-7} m and a viscosity of 10^{-5} Pa s, the asymptotic value of $Nu_d = 3.66$ is considered to be valid.

However, for a given Nusselt number the heat transfer coefficient h is inversely proportional to the channel diameter. Hence, at small sizes, surprisingly high values are obtained [18]. For the given geometry of the anodized membrane pores and a thermal conductivity of $k_{gas} \approx 0.03$ W/(m K) the heat transfer coefficient h reaches a value of

$$h = 3.66 \cdot \frac{k_{gas}}{d} > 5 \times 10^5\ \mathrm{W/(m^2\,K)}. \quad (34)$$

Owing to the small channel dimension, heat transfer in microchannels is much better than in channels of conventional size. For modelling gas micro-heat exchangers, a value of $h = 1000$ W/(m^2 K) is commonly assumed [13], which already represents a rather high value compared to macrochannels. Recently, values up to 35000 W/(m^2 K) have been reported for micro-heat exchangers [19]. With pore diameters smaller than 1 μm, it seems quite probable, that heat transfer coefficients even exceed these values as calculated in Eq. (34).

It has to be noted that for laminar flow in small channels, correct Nusselt numbers are generally smaller than those calculated applying normal size relations [18]. The deviation increases with smaller channels, with a stronger dependence for liquids than for gases. For the Nusselt number Nu defined in Eq. (11), the characteristic length is different from the one used in $\overline{Nu}_d$. With a length to diameter ratio of $L/d = 300$ as present in the pore channels of the applied anodized membranes, applying the macroscale relation (Eq. (34)) results in

$$Nu = \frac{h \cdot \pi d L^2}{A \cdot k_{gas}} = 1.3 \times 10^6. \quad (35)$$

It has to be noted, that the validity of the Nusselt number calculated by applying the macroscale relation defined in Eq. (11), cannot be presumed without any evidence. But even if the macroscale relation cannot be applied and this number has to be reduced by several orders of magnitude, any temperature difference between gas and wall inside the membrane pore would immediately disappear.

3.4. Thermal conductivity and Biot numbers

The thermal conductivity of the membrane material k_{wall} is a material property and a function of temperature. For sintered Al_2O_3 at room temperature, values of $k_{wall} = 33\,W/(m\,K)$ are given, decreasing to 11.4 W/(m K) at $T = 500^\circ$ C [20]. At small material thickness, the thermal conductivity is reported to decrease. For aluminium oxide thin films with a thickness of around 0.3 μm lower values of 3.3 W/(m K) have been determined [21,22], indicating amorphous rather than crystalline structure.

Axial heat conduction is inversely proportional to the channel length. For the small reactor length of $L = 60\,\mu m$ the axial heat conduction is pronounced even for isolating materials. Assuming the high value of $k_{wall} = 20\,W/(m\,8/17/20098/17/20098/17/2009K)$ for the anodized alumina membranes at $T = 200^\circ$ C and the heat transfer coefficient calculated in Eq. (34), the resulting Biot number is

$$Bi = \frac{\epsilon}{1-\epsilon}\frac{h \cdot \pi d L^2}{A \cdot k_{wall}} \approx 500. \tag{36}$$

Smaller values of k_{wall} lead to a further increase of Bi, still indicating a very intensive heat transfer between gas and pore wall compared to heat conduction. On the other hand, a reduced h proportionally reduces Bi. But even if the real heat transfer coefficient is smaller than the one given in Eq. (34) by a factor of 10, the Biot number is still larger than 50, which is still corresponding to very intensive heat transfer between gas and pore wall compared to heat conduction in the wall.

The heat transfer coefficient h_0 in Bi_0, which characterizes heat transfer at the feed side of the membrane, is assumably much smaller than the one for heat transfer in the pores. Even for a high value of $h_0 = 1000\,W/(m^2\,K)$, the Biot number does not exceed a value of

$$Bi_0 = \frac{h_0 \cdot L}{k_{wall}} = 3 \times 10^{-3}, \tag{37}$$

which signifies that due to the small channel length, heat conduction in the pore wall is much larger than heat transfer on the feed side.

3.5. Flow rate and Péclet number

The Péclet number is proportional to the convective heat transfer and thus to the flow rate in the pores. It can be calculated either from the flow rate through a single pore divided by the cross-sectional area of the pore or from the total flow rate divided by the open membrane area, producing equal values. The total standard volumetric flow rates applied in the heat transfer experiments are varied between $Q_{tot} = 1$ and $5\,l_N/min$. This corresponds to molar flow rates of $\dot{n}_{tot} = 0.74 \times 10^{-3}$ to 3.72×10^{-3} mol/s. For a mean molar heat capacity of $c_p = 53\,J/(mol\,K)$ and a mean thermal conductivity of $k_{gas} = 0.03\,W/(m\,K)$ (both valid for ethene at 400 K), the resulting Péclet number range is

$$Pe = \frac{\dot{n}_{tot} \cdot c_p \cdot L}{A_{mem} \cdot k_{gas}} = 0.54 \text{ to } 2.68. \tag{38}$$

These values show that heat convection and heat conduction in the fluid are in the same order of magnitude.

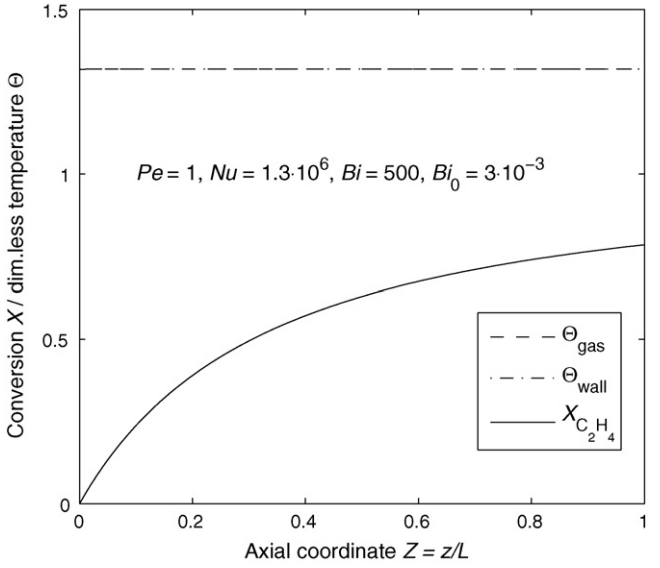

Fig. 6. Axial profiles of conversion, gas and wall temperature for $T_{feed} = 387$ K, $p = 10^5$ Pa, $Q_{tot} = 0.8$ l/min and $x_{C_2H_4} = 0.5$ and parameters determined for the catalytic membrane reactor.

3.6. Temperature profile in catalytic membrane

With the dimensionless quantities determined above for the anodized catalytic membrane reactor, the resulting profiles of temperatures and conversion are illustrated in Fig. 6. The temperatures of gas and wall turn out to be identical and the reactor can be regarded as isothermal.

Parameter variation yields further interesting results: the ratio of Nusselt and Péclet number, commonly referred to as Stanton number St, characterizes the ratio between heat transfer in the pore and heat convection. This ratio can be further described by the internal surface area of the membrane A_{int} and the total pore area ϵA_{mem}, as it is shown in Eq. (39). For values of $St > 1000$, the resulting gas and wall temperature of the investigated system are always in complete agreement and the reactor temperature is constant:

$$St = \frac{Nu}{Pe} = \frac{h \cdot \pi d L^2}{A \cdot k_{gas}} \cdot \frac{A \cdot k_{gas}}{\dot{n}_{tot} \cdot c_p \cdot L} = \frac{h \cdot A_{int}}{\dot{n}_{tot} \cdot c_p} \overset{!}{\geq} 1000, \tag{39}$$

$$A_{int} = \frac{4L}{d} \cdot \epsilon A_{mem}. \tag{40}$$

The correlation implies that the high value for Nu determined in Eq. (35) is not mandatory. For the same Péclet number of $Pe = 1$ a Nusselt number of $Nu = 1000$ is already sufficient to achieve isothermal behavior. Accordingly, for the determined value of $Nu > 10^6$ the flow rate could be increased by orders of magnitude, proportionally increasing Pe, without changing the shape of the temperature profiles.

The second observation concerns the resulting reactor temperature. If Eq. (39) is fulfilled, the permeate temperature, which can be measured experimentally, is equal to both gas and wall temperature along the whole membrane length. All four dimensionless quantities used in the model influence the exact value of the reactor temperature, but these influences can be merged into a single dimensionless quantity, the external Stanton number St_0

$$St_0 = \frac{Nu}{Pe}\frac{Bi_0}{Bi} = \frac{h_0 \cdot (1-\epsilon) A_{mem}}{\dot{n}_{tot} \cdot c_p}. \tag{41}$$

Table 2
Determined St_0 values and resulting reactor temperatures for ethene hydrogenation experiments.

$x_{C_2H_4}$	Q_{tot} [l_N/min]	X	ΔT [K]	$X \cdot \Delta T_{ad}$ [K]	$St_{0,exp}$	$T_{r,exp}$ [K]	$T_{r,sim}$ [K]
0.50	0.80	0.77	185	988	4.34	572	573
0.50	1.50	0.67	161	856	4.33	537	537
0.50	2.50	0.51	99	662	5.70	477	502
0.40	1.00	0.71	155	729	3.72	531	514
0.40	1.88	0.60	132	617	3.68	505	489
0.40	3.13	0.47	87	481	4.55	454	458
0.33	1.20	0.62	104	534	4.12	481	477
0.33	2.25	0.52	96	450	3.71	466	455
0.33	3.75	0.41	65	351	4.38	429	429
0.29	1.40	0.55	72	401	4.57	447	450
0.29	2.63	0.45	66	328	3.95	433	428
0.29	4.38	0.34	49	253	4.15	410	408
				$St_{0,fit}$ =	4.33		

An integral energy balance of the reactor demonstrates that the parameter St_0 is sufficient to describe the reactor temperature:

$$\dot{n}_{tot} c_p (T_{feed} - T_{perm}) - h_0 (1-\epsilon) A_{mem} (T_{wall}(0) - T_{feed}) + \dot{n}_{tot} c_p \Delta T_{ad} X(1) = 0, \quad (42)$$

$$1 - \Theta_{permeate} - St_0 \cdot (\Theta_{wall}(0) - 1) + \Delta\Theta_{ad} \cdot X(1) = 0. \quad (43)$$

If isothermal behavior can be assumed ($St \geq 1000$), the inlet wall temperature $\Theta_{wall}(Z=0)$ and the permeate temperature $\Theta_{permeate}$ are equal and can be replaced by the reactor temperature Θ_r. This resulting reactor temperature is a function of the heat generation term $\Delta\Theta_{ad} \cdot X(1)$ and of St_0:

$$\Theta_r = 1 + \frac{\Delta\Theta_{ad} \cdot X(1)}{1 + St_0}. \quad (44)$$

As $St \geq 1000$ is always fulfilled for the anodized catalytic membrane reactor, the isothermal reactor temperature is only a function of a single unknown parameter, which can be determined experimentally by measuring temperature difference and conversion.

With these correlations it is worth to look once more at the initial temperature profiles with the randomly chosen parameter values. Fig. 5(a) corresponds to relatively large values of $St = St_0 = 10$, whereas Fig. 5(b) represents rather small values of $St = St_0 = 0.1$. Fig. 5(c) results for $St = 1$, $St_0 = 0.1$ and finally Fig. 5(d) corresponds to $St = 1$, $St_0 = 10$. Thus for neither of the four cases, Eq. (39) is fulfilled, causing the non-isothermal profiles. Fig. 5(a) comes closest, whereas Fig. 5(b) is far away from this constraint, producing pronounced temperature profiles. Regarding reactor temperature, Fig. 5(a) and (d) demonstrates effective heat removal with $St_0 = 10$, whereas in the other two cases heat removal is poor with $St_0 = 0.1$, leading to permeate temperatures close to the adiabatic temperature.

4. Experimental model validation

The heat transfer reactor model setup in the previous section is validated experimentally with the aim of determining a correlation for the parameter St_0, which would allow for prediction of reactor temperature and consequently conversion.

The unknown parameter St_0 characterizes heat removal from the membrane. If the system complies with the constraint $St \geq 1000$, St_0 can directly be calculated from measured conversion and temperature difference by means of Eq. (44), which can be transformed to

$$1 + St_0 = \frac{\Delta T_{ad} \cdot X}{T_{permeate} - T_{feed}}. \quad (45)$$

For each of the experiments described in Section 2.2 an individual St_0 can be determined, which exactly predicts the measured temperature (Table 2). The small variation of the individually calculated values suggests that a constant value will lead to satisfying results for the membrane reactor setup under the applied operating parameters. Applying a least squares method, a value of $St_0 = 4.33$ fits the experimental results best.

The theoretical reactor temperatures calculated by means of this constant value are also given in Table 2. The simulated reactor temperatures $T_{r,sim}$ are generally in excellent agreement with the measured temperatures $T_{r,exp}$ (Fig. 7). In eight out of twelve experiments the deviation is lower than 5 K. The largest relative error of 5% is obtained in the third experiment, which also produces the largest deviation in the determination of the reaction kinetics, suggesting an experimental error.

A constant value of St_0 signifies that heat removal from the reactor is not a function of flow rate. For an increasing flow rate $\dot{n}_{tot}$, the heat transfer coefficient h_0 on the feed side increases proportionally. For a rather low standard volume flow rate of $Q_{tot} = 1\,l_N$/min the resulting heat transfer coefficient is $h_0 = 500\,W/(m^2\,K)$, increasing up to $5000\,W/(m^2\,K)$ for 10 l/min.

By means of St_0, which is characteristic for the membrane reactor, a constant heat removal ratio can be specified, defined as the ratio between heat removed from the reactor and heat generated in the reactor, based on Eq. (45):

$$1 - \frac{T_{permeate} - T_{feed}}{\Delta T_{ad} \cdot X} = \frac{St_0}{1 + St_0} = 0.81. \quad (46)$$

This heat removal ratio means that 81% of the heat of reaction is transferred from the reactor to the surrounding module, whereas

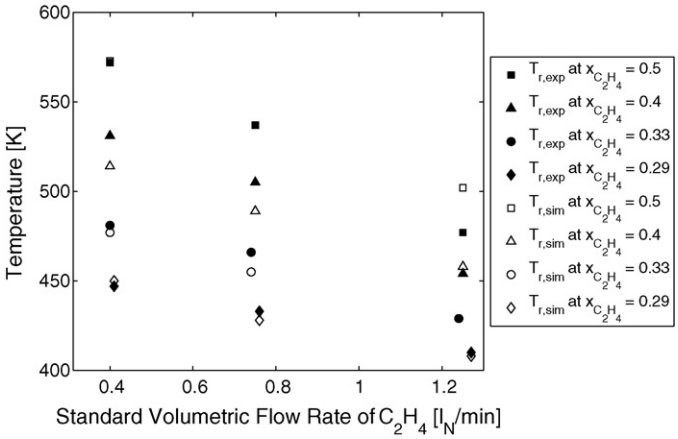

Fig. 7. Comparison between measured reactor temperatures and values calculated by means of the heat transfer reactor model with a constant $St_0 = 4.33$.

19% contribute to the temperature jump at the reactor inlet, i.e. are transported convectively.

The reactor model described in the previous section is well suited to predict the temperature profiles of the flow-through membrane reactor. Due to the small reactor dimensions, isothermal operation will be reached under any operating conditions. In this case, an integral reactor balance allows for calculation of the reactor temperature, which is a function of feed temperature, conversion, adiabatic temperature difference and a constant dimensionless quantity St_0, which accounts for the heat removal from the reactor and is characteristic for the reactor setup under the investigated operating conditions.

Reaction kinetics and consequently the conversion reached in the reactor are a function of the reactor temperature. The steady state reactor temperature in turn is a function of conversion, coupled by the adiabatic temperature rise. As a result, a predictive reactor model has to calculate conversion and reactor temperature simultaneously. The resulting reactor model does not require differential energy balances and represents a boundary value problem, in which the conversion at $Z = 1$ is coupled to the constant reactor temperature according to Eq. (44).

5. Conclusions

A heat transfer model of the catalytic membrane reactor is derived, accounting for heat convection, heat conduction in gas and wall as well as heat transfer inside the catalytic membrane and between membrane and reactor module. All parameters are grouped into four dimensionless quantities *Nu*, *Pe*, *Bi* and Bi_0. If the ratio between *Nu* and *Pe*, the so-called internal Stanton number *St*, becomes larger than 1000, the temperature profiles of gas phase and membrane wall coincide and the reactor can be regarded isothermal. The gas temperature immediately jumps from the lower feed temperature to the constant reactor temperature when entering the catalytic membrane pore. Due to the small reactor dimensions, this requirement is fulfilled in the anodized membrane reactor under any operating conditions. In this case, the heat transfer mechanisms inside the membrane prove to be irrelevant for the resulting membrane temperature, which is exclusively determined by a further dimensionless quantity, the external Stanton number St_0. This parameter results as a combination of the four initial dimensionless numbers and is proportional to the heat transfer coefficient between membrane and reactor module divided by the total flow rate.

Performed ethene hydrogenation experiments suggest that St_0 is nearly constant in the applied range of operating conditions. This implies that for increasing flow rate, the heat transfer coefficient increases proportionally. With this constant parameter characterizing the heat removal ratio from the reactor, the resulting reactor temperature can be predicted satisfactorily in the whole range of performed experiments.

References

[1] V.T. Zaspalis, W. van Praag, K. Keizer, J.G. van Ommen, J.R.H. Ross, A.J. Burggraaf, Reaction of methanol over catalytically active alumina membranes, Applied Catalysis 74 (2) (1991) 205–222.

[2] A. Julbe, D. Farrusseng, C. Guizard, Porous ceramic membranes for catalytic reactors —overview and new ideas, Journal of Membrane Science 181 (1) (2001) 3–20.

[3] J.G. Sanchez Marcano, T.T. Tsotsis, Catalytic Membranes and Membrane Reactors, Wiley–VCH, Weinheim, 2002.

[4] A.G. Dixon, Recent research in catalytic inorganic membrane reactors, International Journal of Chemical Reactor Engineering 1 (R6) (2003) 1–35.

[5] R. Dittmeyer, K. Svajda, M. Reif, A review of catalytic membrane layers for gas/liquid reactions, Topics in Catalysis 29 (1) (2004) 3–27.

[6] R. Schomäcker, A. Schmidt, B. Frank, R. Haidar, A. Seidel-Morgenstern, Membranen als Katalysatorträger, Chemie Ingenieur Technik 77 (5) (2005) 549–558.

[7] T. Westermann, T. Melin, Flow-through catalytic membrane reactors—principles and applications, Chemical Engineering and Processing: Process Intensification 48 (1) (2009) 17–28.

[8] T. Westermann, T. Melin, Single flow-through catalytic membrane microchannel reactor for intensified heterogeneous catalysis: characterisation and application to hydrogenation of ethyne, in: European Congress of Chemical Engineering (ECCE-6), Copenhagen, Denmark, 2007, pp. 807–808.

[9] H. Masuda, H. Yamada, M. Satoh, H. Asoh, M. Nakao, T. Tamamura, Highly ordered nanochannel-array architecture in anodic alumina, Applied Physics Letters 71 (19) (1997) 2770–2772.

[10] O. Jessensky, F. Müller, U. Gosele, Self-organized formation of hexagonal pore arrays in anodic alumina, Applied Physics Letters 72 (10) (1998) 1173–1175.

[11] C. Knösche, Wärmeabfuhr und Rückvermischung in mikrostrukturierten Apparaten, Chemie Ingenieur Technik 77 (11) (2005) 1715–1722.

[12] Y. Xu, B. Platzer, Konzepte zur Simulation katalysierter Reaktionen in Mikroreaktoren mit Mesoporen im Wandbereich, Chemie Ingenieur Technik 73 (1–2) (2001) 27–39.

[13] T. Stief, O.-U. Langer, K. Schubert, Numerische Untersuchungen zur optimalen Wärmeleitfähigkeit in Mikrowärmeübertragerstrukturen, Chemie Ingenieur Technik 70 (12) (1998) 1539–1544.

[14] P.V. Danckwerts, Continuous flow systems: distribution of residence times, Chemical Engineering Science 2 (1) (1953) 1–13.

[15] A.N.R. Bos, E.S. Botsma, F. Foeth, H.W.J. Sleyster, K.R. Westerterp, A kinetic study of the hydrogenation of ethyne and ethene on a commercial Pd/Al_2O_3 catalyst, Chemical Engineering and Processing 32 (1) (1993) 53–63.

[16] A.N.R. Bos, K.R. Westerterp, Mechanism and kinetics of the selective hydrogenation of ethyne and ethene, Chemical Engineering and Processing 32 (1) (1993) 1–7.

[17] V. Gnielinski, VDI-Wärmeatlas, Springer-Verlag, Berlin Heidelberg, 2006 (Ch. Wärmeübertragung bei der Strömung durch Rohre, p. Ga 3.1.1.).

[18] M.-N. Sabry, Scale effects on fluid flow and heat transfer in microchannels, IEEE Transactions on Components and Packaging Technologies 23 (3) (2000) 562–567.

[19] A. Stankiewicz, Re-engineering the Chemical Processing Plant: Process Intensification, 1st ed., no. 98 in Chemical Industries, Marcel Dekker, Inc., 2004.

[20] R.G. Munro, Evaluated material properties for a sintered alpha-alumina, Journal of the American Ceramic Society 80 (8) (1997) 1919–1928.

[21] R. Kato, A. Maesono, R.P. Tye, Thermal conductivity measurement of submicron-thick films deposited on substrates by modified ac calorimetry (laser-heating Ångstrom method), International Journal of Thermophysics 22 (2) (2001) 617–629.

[22] S.-Y. Bai, Z.-A. Tang, Z.-X. Huang, J. Yu, J.-Q. Wang, Thermal conductivity measurement of submicron-thick aluminium oxide thin films by a transient thermo-reflectance technique, Chinese Physics Letters 25 (2) (2008) 593–596.